

# Hybrid star structure with the Field Correlator Method

G. F. Burgio<sup>1</sup> and D. Zappalà<sup>1</sup>

<sup>1</sup> INFN Sezione di Catania, Via Santa Sofia 64, 95123 Catania, Italy

Received: date / Revised version: date

**Abstract.** We explore the relevance of the color-flavor locking phase in the equation of state (EoS) built with the Field Correlator Method (FCM) for the description of the quark matter core of hybrid stars. For the hadronic phase, we use the microscopic Brueckner-Hartree-Fock (BHF) many-body theory, and its relativistic counterpart, i.e. the Dirac-Brueckner (DBHF). We find that the main features of the phase transition are directly related to the values of the quark-antiquark potential  $V_1$ , the gluon condensate  $G_2$  and the color-flavor superconducting gap  $\Delta$ . We confirm that the mapping between the FCM and the CSS (constant speed of sound) parameterization holds true even in the case of paired quark matter. The inclusion of hyperons in the hadronic phase and its effect on the mass-radius relation of hybrid stars is also investigated.

**PACS.** 25.75.Nq Quark deconfinement, quark-gluon plasma production, and phase transitions – 26.60.-c Nuclear matter aspects of neutron stars – 97.60.Jd Neutron stars

## 1 Introduction

The possible appearance of quark matter (QM) in the interior of massive neutron stars (NS) is currently one of the main theoretical issues in the physics of compact stars [1]. The existence of two NS of about two solar masses [2, 3] has been confirmed by recent observations. Based on a microscopic nucleonic equation of state (EoS), one expects that in such heavy NS the central particle density reaches values larger than  $1/fm^3$ , where in fact quark degrees of freedom are expected to appear at a macroscopic level. Unfortunately, while the microscopic theory of the nucleonic EoS has reached a high degree of sophistication [4, 5, 6, 7, 8], the QM EoS is still poorly known at zero temperature and at the high baryonic density appropriate for NS. In fact the essential theoretical tool, i.e. lattice formulation of the quantum chromodynamics (QCD) is inapplicable at large baryon densities and small temperature due to the so-called Sign Problem [9], and this is due to its complicated nonlinear and nonperturbative nature. On the other hand, in the large temperature and small density region lattice QCD simulations have provided controlled results for the EoS as well as for the nature of the transition [10, 11].

The mass of a NS can be calculated by solving the Tolman-Oppenheimer-Volkoff (TOV) equations with the relevant EoS as input. The hybrid EoS including both hadronic matter and QM is usually obtained by combining EoSs of hadronic matter and QM within individual theories/models.

Continuing a set of investigations using different quark models [12, 13, 14, 15], recently we have explored the nature of the phase transition with the Field Correlator Method (FCM) model of quark matter [16, 17, 18], which in principle is able to cover the full temperature-chemical potential plane. In our previous papers [19, 20], we tested the FCM model by comparing the results for the neutron star masses with the existing phenomenology, which puts strong constraints on the parameters of the model, i.e. the quark-antiquark potential  $V_1$  and the gluon condensate  $G_2$ .

Recently, we found that the FCM model can be expressed in the language of the "Constant Speed of Sound" (CSS) parameterization [21, 22], and we showed how its parameters can be mapped on to the CSS parameter space. We remind that the CSS scheme is a general parameterization suitable for expressing experimental constraints in a model-independent way and for classifying different models of quark matter and establishing connections among them. It is applicable to high-density equations of state for which: (a) there is a sharp interface between nuclear matter and quark matter, (b) the speed of sound in the high-density matter is pressure-independent in the range between the first-order transition pressure up to the maximum central pressure of neutron stars. Given the nuclear matter EoS  $\epsilon_{\text{NM}}(p)$ , the high-density EoS can be expressed as

$$\epsilon(p) = \begin{cases} \epsilon_{\text{NM}}(p) & p < p_{\text{trans}} \\ \epsilon_{\text{NM}}(p_{\text{trans}}) + \Delta\epsilon + c_{\text{QM}}^{-2}(p - p_{\text{trans}}) & p > p_{\text{trans}} \end{cases} \quad (1)$$

where the three parameters: the pressure  $p_{trans}$  of the transition, the discontinuity in energy density  $\Delta\epsilon$  at the transition, and the speed of sound  $c_{QM}$  characterize completely the high-density phase.

In this work we elaborate more on that point by extending the FCM model in order to include the color superconductivity through the color-flavor locking (CFL) mechanism, which mimics an explicit dependence of the gluon condensate  $G_2$  on the quark chemical potential, as initially studied in ref.[20]. We find that the value of the hybrid star maximum mass depends strongly on the FCM model parameters, i.e.  $V_1$ ,  $G_2$  and the gap  $\Delta$ . We also find that the mapping on to the CSS parameterization still holds true when including the CFL phase, though the parameter region explored depends on the value of the gap  $\Delta$ . We also pay special attention to the analysis of the hadron-quark phase transition when hyperons are included in the hadronic phase. In fact, given the strong softening of the EoS when hyperons are included, it has been often found that no quark matter phase transition can take place [13,15].

This paper is organized as follows. In the next section we briefly review the EoS of the hadronic sector, particularly the BHF and DBHF microscopic approaches. In Sect. 3 we discuss the quark matter EoS, and in Sect. 3.1 we illustrate the FCM at finite density, with the inclusion of the color-flavor locking effect in Sec. 3.2. Sect. 4 contains numerical results, with some details of the EoS for neutron star matter and the hadron-quark phase transition in Sect. 4.1. In Sect. 4.2 we discuss the mass-radius-central density relation for hybrid stars, and the FCM mapping onto the CSS parameterization. Effects due to the inclusion of hyperons are explored in Sect. 4.3. Finally we draw our conclusions in Sect.5.

## 2 The BHF and DBHF EoS of Nuclear Matter

Empirical properties of infinite nuclear matter can be calculated using many different theoretical approaches. The amount of experimental and observational data obtained in the last few years, and the intense theoretical efforts aimed at their interpretation, call for a firm microscopic approach to the modeling of the Equation of State (EoS). In a microscopic approach, the only input required is a realistic free nucleon-nucleon (NN) interaction with parameters fitted to NN scattering phase shifts in different partial wave channels, and to properties of the deuteron. In this paper we adopt the non-relativistic Brueckner-Bethe-Goldstone (BBG) method [23] and its relativistic counterpart, the Dirac-Brueckner-Hartree-Fock (DBHF) approximation [24].

The Brueckner-Bethe-Goldstone (BBG) theory is based on a linked cluster expansion of the energy per nucleon of nuclear matter (see Ref. [23], chapter 1 and references therein). The basic ingredient in this many-body approach is the Brueckner reaction matrix  $G$ , which is the solution of the Bethe-Goldstone equation

$$G[\rho; \omega] = v + \sum_{k_a k_b} v \frac{|k_a k_b\rangle Q \langle k_a k_b|}{\omega - e(k_a) - e(k_b)} G[\rho; \omega], \quad (2)$$

where  $v$  is the bare NN interaction,  $\rho$  is the nucleon number density, and  $\omega$  the starting energy. The single-particle energy  $e(k)$  (assuming  $\hbar=1$ ),

$$e(k) = e(k; \rho) = \frac{k^2}{2m} + U(k; \rho), \quad (3)$$

and the Pauli operator  $Q$  determine the propagation of intermediate baryon pairs. The Brueckner-Hartree-Fock (BHF) approximation for the single-particle potential  $U$  using the *continuous choice* is

$$U(k; \rho) = \text{Re} \sum_{k' \leq k_F} \langle kk' | G[\rho; e(k) + e(k')] | kk' \rangle_a, \quad (4)$$

where the subscript “a” indicates antisymmetrization of the matrix element. Due to the occurrence of  $U(k)$  in Eq. (3), the above equations constitute a coupled system that has to be solved in a self-consistent manner for several momenta of the particles involved, at the considered densities. In the BHF approximation the energy per nucleon is

$$\frac{E}{A} = \frac{3}{5} \frac{k_F^2}{2m} + \frac{1}{2\rho} \sum_{k, k' \leq k_F} \langle kk' | G[\rho; e(k) + e(k')] | kk' \rangle_a. \quad (5)$$

In this scheme, the only input quantity we need is the bare NN interaction  $v$  in the Bethe-Goldstone equation (1). It has been shown that the nuclear EoS can be calculated with good accuracy in the Brueckner two hole-line approximation with the continuous choice for the single-particle potential, since the results in this scheme are quite close to the calculations which include also the three hole-line contribution [25,26,27]. The dependence on the NN interaction, also within other many-body approaches, has been systematically investigated in Ref.[7].

However, it is commonly known that non-relativistic calculations, based on purely two-body interactions, do not reproduce correctly the saturation point of symmetric nuclear matter, and that three-body forces (TBF) are needed to correct this deficiency. For that, TBF are reduced to a density dependent two-body force by averaging over the position of the third particle, assuming that the probability of having two particles at a given distance is reduced according to the two-body correlation function [4,6]. Recently, it has been shown that the role of TBF is greatly reduced if the NN potential is based on a realistic constituent quark model [28].

In this work we will illustrate results obtained using a phenomenological approach to the TBF, which is based on the so-called Urbana model, and consists of an attractive term due to two-pion exchange with excitation of an intermediate  $\Delta$  resonance, and a repulsive phenomenological central term [29,30]. Within the BHF approach, those TBF produce a shift of about +1 MeV in energy

and  $-0.01 \text{ fm}^{-3}$  in density. This adjustment is obtained by tuning the two parameters contained in the TBF, and was performed to get an optimal saturation point.

At present the theoretical status of microscopically derived TBF is still quite rudimentary, however a tentative approach has been proposed using the same meson-exchange parameters as the underlying NN potential. Results have been obtained with the Argonne  $v_{18}$ , the Bonn B, and the Nijmegen 93 potentials [8,31].

In the past years, the BHF approach has been extended in order to include the hyperon degrees of freedom [32,33], which play an important role in the study of neutron star matter. In fact, hyperons are expected to appear in beta-stable matter already at relatively low densities of about twice nuclear saturation density, thus producing a softening of the EoS. If this is the case, the existence of heavy NS would question the presence of hyperons in their interior, thus requiring alternative scenarios. It is therefore of great importance to carry out accurate theoretical calculations of hypernuclear matter starting from the available experimental information on both nucleon and hyperon interactions. In the Brueckner scheme, the fundamental input are the hyperon-nucleon (YN), and hyperon-hyperon (YY) potentials, besides realistic NN potentials. There exist several YN potentials fitted to scattering data, i.e. NSC89 [34], NSC97 [35], and ESC08 [36], while the YY potentials have presently to be considered rather uncertain or unknown, which is basically due to the lack of appropriate experimental data. In the Brueckner approach, very low maximum masses of hyperon stars, below  $1.4 M_\odot$  ( $M_\odot = 2 \times 10^{33} \text{ g}$ ) were always found.

The relativistic framework is the one on which the nuclear EoS should be ultimately based. The best relativistic treatment developed so far is the Dirac-Brueckner (DBHF) approach [24]. The DBHF method can be developed in analogy with the non-relativistic case, i.e. the nucleon inside the nuclear medium is viewed as a dressed particle in consequence of its two-body interaction with the surrounding nucleons. The two-body correlations are described by introducing the in-medium relativistic  $G$ -matrix. The DBHF scheme can be formulated as a self-consistent problem between the single particle self-energy  $\Sigma$  and the  $G$ -matrix. It has been shown that the DBHF treatment is equivalent [37] to introducing in the nonrelativistic BHF the three-body force corresponding to the excitation of a nucleon-antinucleon pair, the so-called Z-diagram [38], which is repulsive at all densities, and consequently produces a saturating effect. Actually, including in BHF only these particular TBF, one gets results close to DBHF calculations, see Ref.[39]. Generally speaking, the DBHF gives in general a better saturation point than BHF, and the corresponding EoS turns out to be stiffer above saturation than the one calculated from the BHF + TBF method. In the relativistic context the only NN potentials which have been developed are the ones of one-boson exchange (OBE) type. In the calculations shown here the Bonn A potential is used [24].

## 3 The quark matter EoS

### 3.1 The Field Correlator Method

The approach we follow to describe the quark matter EoS was introduced in [16,17,18] ; see ref.[40] for a review. For our purposes, we are specifically interested in the extension of this approach to finite baryon density and temperature, and all we need is the expression of the pressure as a function of the EoS thermodynamical parameters, i.e. the baryon chemical potential  $\mu_B$  and the temperature  $T$ . This is derived in [41,42,43], and below we report its explicit form. The full pressure,  $P_{qq}$ , is the sum of the gluon,  $P_g$ , the quark,  $P_q$ , and the vacuum,  $P_v$ , contributions

$$P_{qq} = P_g + \sum_{j=u,d,s} P_q^j + P_v \quad (6)$$

where the sum is extended to the three light quark flavors. The gluon pressure is

$$P_g = \frac{8T^4}{3\pi^2} \int_0^\infty d\chi \chi^3 \frac{1}{\exp(\chi + \frac{9V_1}{8T}) - 1} \quad (7)$$

while the quark pressure for each single flavor with mass  $m_q$  and chemical potential  $\mu_q$ , is

$$P_q = \frac{T^4}{\pi^2} \left[ \phi_\nu\left(\frac{\mu_q - V_1/2}{T}\right) + \phi_\nu\left(-\frac{\mu_q + V_1/2}{T}\right) \right] \quad (8)$$

where

$$\phi_\nu(a) = \int_0^\infty du \frac{u^4}{\sqrt{u^2 + \nu^2}} \frac{1}{(\exp[\sqrt{u^2 + \nu^2} - a] + 1)}, \quad (9)$$

being  $\nu = m_q/T$ . Finally  $P_v$ , which represents the pressure difference between the vacua in the deconfined and confined phases, is given by

$$P_v = -\frac{(11 - \frac{2}{3}N_f) G_2}{32} \frac{G_2}{2} \quad (10)$$

where the number of light flavors in our case is  $N_f = 3$ .

Then, once the quark chemical potentials are related to the baryon chemical potential  $\mu_B$ , the full pressure  $P_{qq}$  is defined in terms of the two parameters  $V_1$  and  $G_2$  appearing in Eqs. (7-10), where  $V_1$  indicates the large distance static  $q\bar{q}$  potential and  $G_2$  is the gluon condensate. The former is essentially of nonperturbative nature and can be expressed in terms of an integral of a fundamental QCD correlator [41,42,43]; however there is no direct measurement of its value. The latter is known from QCD sum rules [44,45],  $G_2 = \langle \frac{\alpha_s}{\pi} G_{\mu\nu}^a G^{a\mu\nu} \rangle = 0.012 \text{ GeV}^4$ , although an uncertainty of about 50% affects this estimate.

It is also interesting to notice that  $G_2$  appears only in the vacuum contribution to the pressure, and  $P_v$  in Eq. (10) has the same role of the bag constant of the MIT bag model. Moreover, if one turns off the potential  $V_1$ , the quark pressure  $P_q$  becomes the pressure of free quarks, and in this case the FCM model reduces to the simplest

version of the bag model. Therefore  $V_1$  can be regarded as the main correction to the free quarks dynamics inside the bag.

In addition to the poor knowledge of the phenomenological values of  $V_1$  and  $G_2$ , it is reasonable to expect some dependence of these parameters on the thermodynamical variables  $\mu_B$  and  $T$ . In fact, for the  $T$  dependence some indications can be obtained from the analysis of the deconfinement phase transition, which is supported by lattice calculations. For instance, the fact that the gluon condensate  $G_2$  is substantially  $T$  independent except at  $T_c$ , where it is sharply reduced by one half [46,47], was already accounted for in the vacuum pressure difference of the two phases derived in [41] and reported in Eq. (10).

As far as  $V_1$  is concerning, by making use of a relation among  $V_1$ ,  $G_2$  and the critical temperature  $T_c$  derived in [41,42], the estimate  $V_1(T_c) = 0.5$  GeV was obtained in [48] with  $G_2 \simeq 0.004$  GeV<sup>4</sup>, which reduces to  $V_1(T_c) \sim 0.15$  GeV when  $G_2 = 0.012$  GeV<sup>4</sup>. The more accurate analysis performed in [20] shows that the large set of lattice data on the interaction measure points toward a value of  $V_1(T_c)$  around  $0.5 - 0.6$  GeV when  $G_2 = 0.012$  GeV<sup>4</sup>. Then, according to the  $T$  dependence of  $V_1$  presented in [41,42],  $V_1(T_c) \sim 0.5 - 0.6$  GeV would correspond to higher values of this parameter at zero temperature  $V_1(T = 0) \simeq 0.8 \div 0.9$  GeV [48].

These results are valid at zero baryon density, while the dependence of the two parameters on  $\mu_B$  is more relevant in the study of the composition of the NS and, in fact in our analysis we work by taking  $T = 1$  MeV, that in practice is equivalent to vanishing temperature. Actually the potential  $V_1$  is expected to be independent on the chemical potential at least at very small chemical potentials [42]. However, in [20] it was suggested that, as at large baryon density the antiquark number becomes negligible and the quark-quark interaction relevant, one should replace the quark-antiquark with the quark-quark potential and this should result in a reduction of the parameter  $V_1$  which represents an effective measure of the size of the interactions.

Therefore, having no strong indications on the specific dependence of the potential  $V_1$  on  $\mu_B$ , it is more significant to leave  $V_1$  as a free parameter in our analysis of the NS composition. We discuss the problem of the dependence of  $G_2$  on the chemical potential in the next subsection.

### 3.2 The color-flavor locking effect

In ref.[20] the dependence of  $G_2$  on  $\mu_B$  was explicitly studied by introducing a particular ansatz for  $G_2(\mu_B)$ , which was based on previous analysis of the expectation of the gluon condensate in dense nuclear matter [49,50,51] and in two-color,  $N_c = 2$ , quantum chromodynamics [52,53]. In particular, in [52,53] it is shown that the explicit form obtained for  $G_2(\mu_B)$  (it starts as a decreasing function at small  $\mu_B$  and turns into an increasing function at larger  $\mu_B$ , with a minimum between these two regions) is related to the effect of diquark pairing and the appearance of a mass gap. In fact, at a qualitative level

this effect presents strong similarities with the occurrence of the color-flavor locking (CFL) superconductive mechanism in standard  $N_c = 3$  QCD [54,55], which, as far as the total pressure of the quark system is concerned, induces an additional pressure term parameterized by a gap  $\Delta$ . Clearly, this new pressure term has an essential role in shaping the  $\mu_B$  dependence of the gluon condensate  $G_2$ , which eventually has the same qualitative features of the curve derived in [53].

Therefore, due to the unavoidable arbitrariness associated to the choice of the ansatz for  $G_2(\mu_B)$  encountered in [20], rather than following that approach we prefer to adopt here a more realistic point of view, i.e. keeping  $G_2(\mu_B = 0)$  as a free parameter, which is a necessary ingredient to set the pressure difference between the confined and deconfined phase, and adding to the full FCM pressure  $P_{qg}$  the additional contribution due to CFL.

The presence of color-flavor locked quark matter is expected at very high  $\mu_B$ , and it is realized through quark-quark pairing under the constraint that the densities of the three flavors, up, down and strange, are equal [55,56,57,58]. The global effect of this pairing on the pressure is the presence of the additional term

$$P_{cfl} = \frac{\Delta^2 \mu_B^2}{3\pi^2} \quad (11)$$

only when the chemical potential is greater than  $\mu_B = 3m_s^2/(4\Delta)$  and the gap  $\Delta$  is expected to be in the range  $10 - 100$  MeV in the region of interest of  $\mu_B$  for the NS. Finally the total pressure of the quark matter phase is obtained by adding  $P_{cfl}$  to  $P_{qg}$  given in Eq. (6), and is treated as a function of the baryon chemical potential  $\mu_B$  with three free parameters, namely the potential  $V_1$  and the gluon condensate  $G_2$ , coming from the FCM model, and the gap  $\Delta$ , due to the CFL pairing.

## 4 Numerical Results

### 4.1 EoS of dense matter in beta equilibrium

In order to study the structure of NS, we have to calculate the composition and the EoS of cold, neutrino-free, charge-neutral, and beta-stable matter, characterized by two degrees of freedom  $\mu_B$  and  $\mu_e$ , the baryon and charge chemical potentials. The corresponding equations are

$$\mu_i = b_i \mu_B - q_i \mu_e, \quad \sum_i \rho_i q_i = 0, \quad (12)$$

$b_i$  and  $q_i$  denoting baryon number and charge of the particle species  $i = n, p, e, \mu$  in the hadron phase and  $i = u, d, s, e, \mu$  in the quark phase, respectively.

As far as the hadronic phase is concerning, the Brueckner calculation yields the energy density of baryon/lepton matter as a function of the different partial densities,

$$\epsilon(\rho_n, \rho_p, \rho_e, \rho_\mu) = (\rho_n m_n + \rho_p m_p) + (\rho_n + \rho_p) \frac{E}{A}(\rho_n, \rho_p)$$

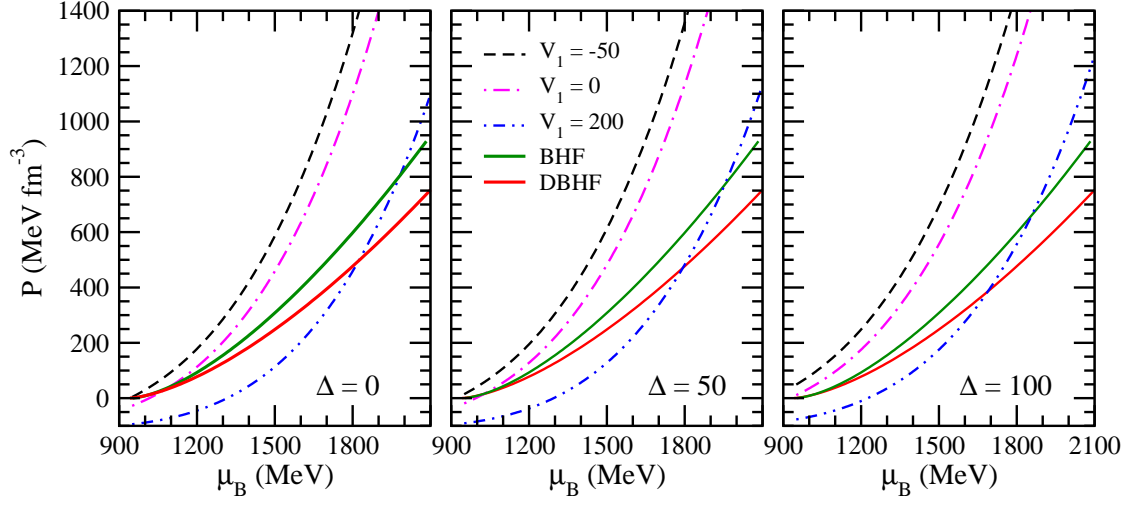


**Fig. 1.** (Color online) The pressure is displayed as a function of the baryon chemical potential  $\mu_B$  for the FCM quark matter and the purely hadronic matter. All calculations for FCM have been performed for  $G_2 = 0.006 \text{ GeV}^4$ , and several values of  $V_1$  have been chosen. The solid curves represent the BHF (green) and DBHF (red) EoS. Each panel shows results for different values of the gap  $\Delta$ , i.e. 0, 50, and 100 MeV.

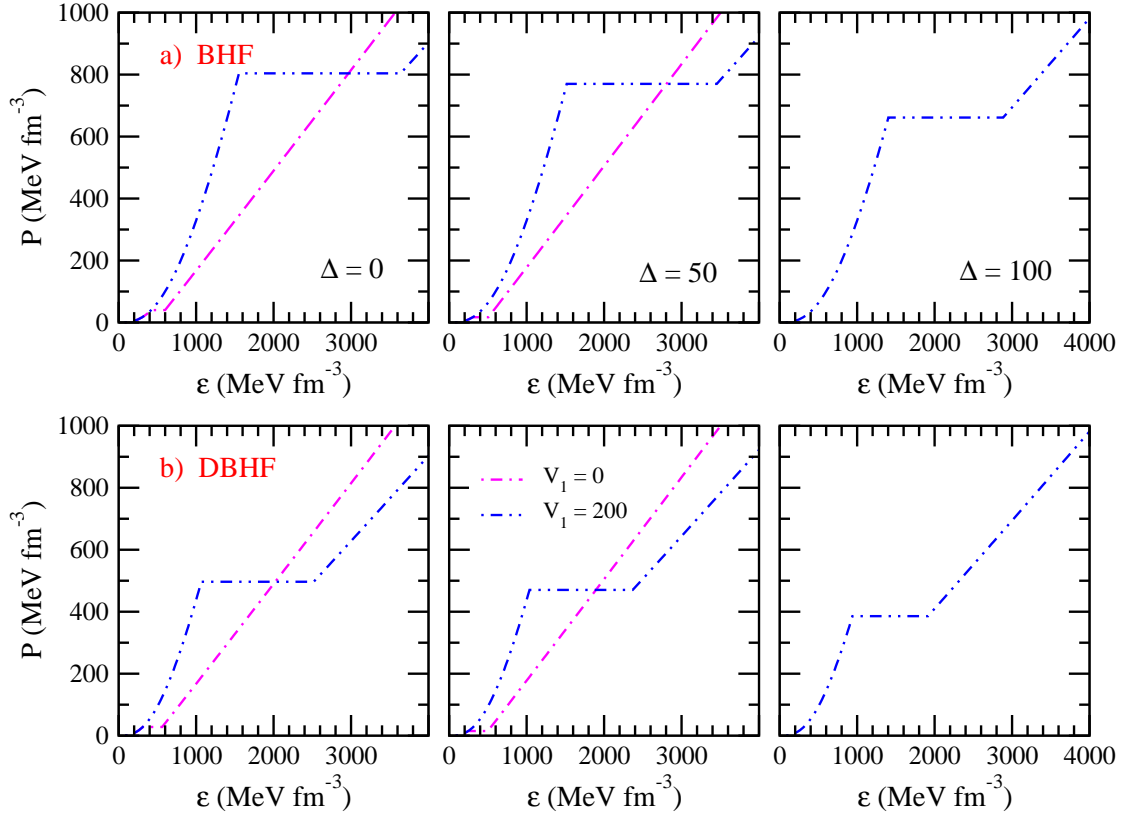


**Fig. 2.** (Color online) The pressure is displayed vs. the energy density for  $V_1 = 0$  (magenta curves) and  $V_1 = 200$  (violet) using as hadronic EoS the BHF (upper panels) and the DBHF (lower panels). All calculations for FCM have been performed for  $G_2 = 0.006 \text{ GeV}^4$ . The left, middle and right panels correspond to the values  $\Delta = 0, 50, 100 \text{ MeV}$  respectively.

$$\begin{aligned}
& + \rho_\mu m_\mu + \frac{1}{2m_\mu} \frac{(3\pi^2 \rho_\mu)^{5/3}}{5\pi^2} \\
& + \frac{(3\pi^2 \rho_e)^{4/3}}{4\pi^2}, \quad (13)
\end{aligned}$$

where we have used ultrarelativistic and nonrelativistic approximations for the energy densities of electrons and muons, respectively. In this study, we adopt the parabolic approximation for  $E/A$  [4]. Once the energy density is known (Eq. (13)), the various chemical potentials (of the species  $i = n, p, e, \mu$ ) can be computed straightforwardly,

$$\mu_i = \frac{\partial \epsilon}{\partial \rho_i}, \quad (14)$$

and the equations for beta-equilibrium (12) allow one to determine the equilibrium composition  $\{\rho_i\}$  at given baryon density  $\rho$  and finally the EoS,

$$P = \rho^2 \frac{d}{d\rho} \frac{\epsilon(\{\rho_i(\rho)\})}{\rho} = \rho \frac{d\epsilon}{d\rho} - \epsilon = \rho \mu_B - \epsilon. \quad (15)$$

As far as the quark phase is concerning, it is necessary to define the relations among the various  $\mu_q$  that appear in Eq. (8) and the variable  $\mu_B$ . For this purpose we must distinguish two cases, one with  $\Delta = 0$  and the other with  $\Delta \neq 0$ . In the first case one has  $P_{cfl} = 0$  and the corresponding EoS for quark matter is determined by the conditions of  $\beta$ -equilibrium and charge neutrality and baryon number conservation, as expressed by Eq.(12). It is then sufficient to express each  $\mu_q$  in terms of one single variable, namely  $\mu_B$ . In the second case, with  $\Delta \neq 0$ , the charge neutrality condition is realized in a peculiar way [56]. In fact, CFL pairing occurs if the number densities of the three flavors are equal

$$\rho_u = \rho_d = \rho_s \quad (16)$$

which implies vanishing electron density,  $\rho_e = 0$ , in order to maintain full charge neutrality. As explained in [56], Eqs. (16) with non vanishing strange quark mass,  $m_s \neq 0$ , are acceptable only if  $\mu_e \neq 0$ , but in any case they allow us to determine each single  $\mu_q$  in terms of  $\mu_B$ . Therefore, each time we consider the case with  $\Delta \neq 0$ , we use the specific condition in Eqs. (16) to express  $\mu_q$  in Eq. (8) in terms of  $\mu_B$ .

Let us now discuss the main features of the hadron-quark phase transition, which we assume to be first-order, thus performing the Maxwell construction. Fig. 1 shows numerical results for the pressure as a function of the baryon chemical potential  $\mu_B$  in the hadronic matter and quark matter in beta equilibrium. In particular, the green (red) solid curves represent the BHF (DBHF) EoS, whereas the remaining curves are the results for the FCM model with different choices of the quark-antiquark potential  $V_1$  (expressed in MeV). In the left, middle and right panels the value assumed for the gap  $\Delta$  is respectively equal to 0, 50 and 100 MeV. All calculations shown in Fig. 1 are performed taking  $G_2 = 0.006 \text{ GeV}^4$ . We notice that with increasing the value of  $V_1$  the quark matter EoS becomes

stiffer and therefore the transition point is shifted to larger values of the chemical potential, hence of the baryon density. However, the exact value depends also on the stiffness of the hadronic EoS at those densities. In this case, being the DBHF EoS stiffer than the BHF, the transition takes place at smaller values of the density. We notice that the transition point is affected also by the value of the gap  $\Delta$ , a larger value of which implies a softer quark matter EoS and therefore a shift towards smaller  $\mu_B$ . Moreover, no phase transition occurs for negative values of  $V_1$ .

The resulting EoS, for the several cases discussed, is displayed in Fig. 2, where one can directly read off the phase transition between hadron matter and quark matter under the Maxwell construction. We notice that the phase transition is allowed only for  $V_1 \geq 0$ , and that the width of the plateau is directly related to  $\Delta$ . In the case  $V_1 = 0$  (magenta curve) the phase transition takes place at very low value of the density, the plateau is quite small and the pure quark matter phase starts at density about 3 times normal nuclear matter density. By increasing  $V_1$  the phase transition is shifted to larger values of the energy density.

## 4.2 Hybrid star structure

Once the EoS of the hybrid star matter is known, one can use the Tolman-Oppenheimer-Volkoff [59] equations for spherically symmetric NS:

$$\frac{dp}{dr} = -\frac{Gm\epsilon}{r^2} \frac{(1+p/\epsilon)(1+4\pi r^3 p/m)}{1-2Gm/r}, \quad (17)$$

$$\frac{dm}{dr} = 4\pi r^2 \epsilon, \quad (18)$$

where  $G$  is the gravitational constant and  $m(r)$  is the enclosed mass within a radius  $r$ . Given a starting energy density  $\epsilon_c$ , one integrates these equations until the surface  $r = R$ , and the gravitational mass is obtained by  $M_G = m(R)$ . The EoS needed to solve the TOV equations is taken from the neutron star matter calculations discussed above, and matched with the crust EoS, which has been taken from Refs. [60].

As is well known, the mass of the NS has a maximum value as a function of radius (or central density), above which the star is unstable against collapse to a black hole. The value of the maximum mass depends on the EoS, so that the observation of a mass higher than the maximum mass allowed by a given EoS simply rules out that EoS. This is illustrated in Fig. 3, where the relation between mass and radius (left panel) and central density (right panel) in units of the saturation density  $\rho_0 = 0.17 \text{ fm}^{-3}$  is displayed. Results are plotted for the case in which the BHF EoS is used for hadronic matter. In Fig. 3 we plot several cases obtained for different values of  $V_1$ ,  $G_2$  and  $\Delta$  and in this example the largest value of the maximum mass is observed for large values of  $V_1 = 200 \text{ MeV}$ ,  $\Delta = 100$  and  $G_2 = 0.01$ , and it is compatible with the largest mass observed up to now, i.e.  $(2.01 \pm 0.04)M_\odot$  in PSR J0348+0432 [3].

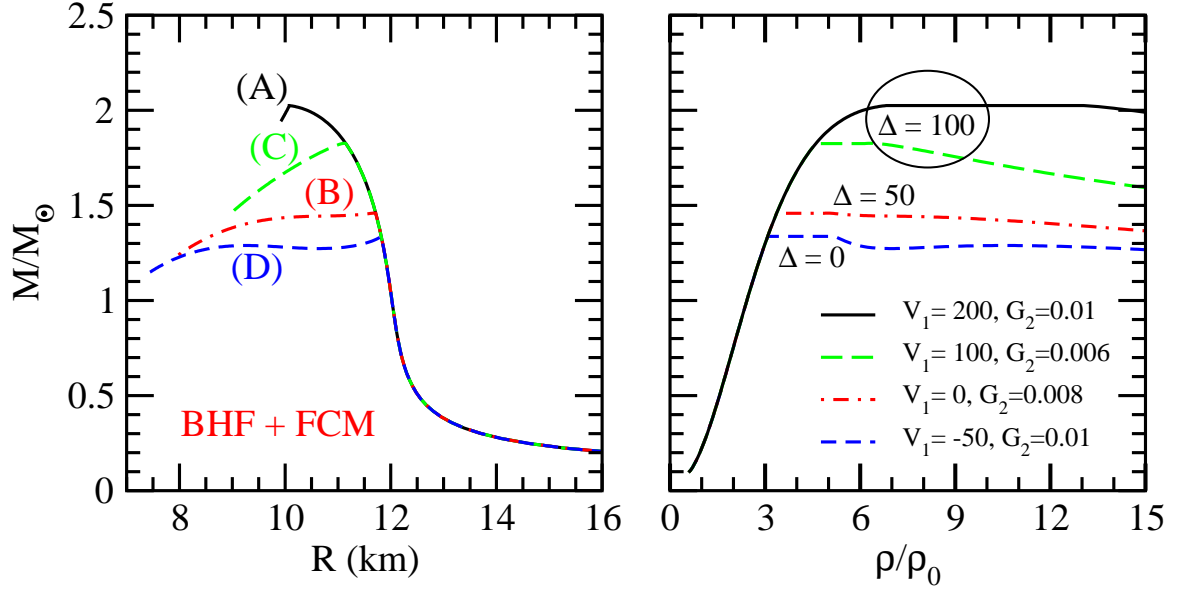


**Fig. 3.** (Color online) The mass as function of the radius (left panel) and the central density (right panel) is displayed for several values of  $V_1$ ,  $G_2$  and  $\Delta$ . The BHF EoS is used for the hadronic phase. The labels (A), (B), (C) and (D) indicate the specific topologies of the hybrid star branch.

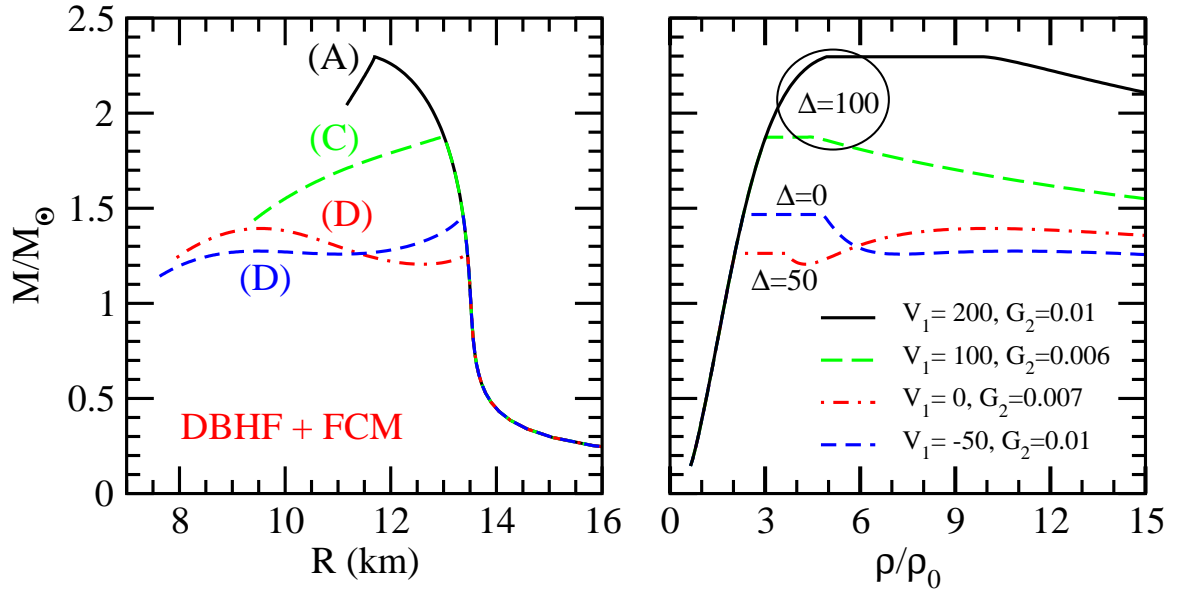


**Fig. 4.** Same as Fig.3, but for the DBHF EoS.

Recently, it has been shown in ref. [22] that the FCM equation of state can be accurately represented by the so-called CSS parameterization. The basic ansatz is that a sharp phase transition occurs to a high-density phase, where the speed of sound is density-independent. As already discussed in ref.[21], in all models of nuclear/quark matter one can find the four topologies of the mass-radius curve for compact stars: the hybrid branch may be connected to the nuclear branch (C), or disconnected (D), or

both may be present (B) or neither (A). We will discuss in detail the FCM mapping onto the CSS parameterization in the next subsection. Here we limit ourselves to use the same labels in Figs. 3 and 4 in order to indicate the topology of the mass-radius curve, which is strongly related to the values of the pressure and energy density at the transition point, and to the energy density discontinuity. In the framework of the FCM model, the topology is related to the chosen values of  $V_1$ ,  $G_2$  and  $\Delta$ . Using

Fig. 1 as a guide, we can obtain various topologies just changing  $V_1$ ,  $G_2$  and  $\Delta$ . For example, when combining FCM quark matter to the BHF nuclear matter we find that, for unpaired quark matter and  $V_1 = -50$  MeV, the lowest transition point can be obtained when  $G_2 > 0.006$  GeV<sup>4</sup>. In Fig. 3 the corresponding mass-radius relation, obtained with  $G_2 = 0.01$  GeV<sup>4</sup> is displayed by the blue dashed line, which exhibits a branch of stable hybrid stars disconnected (D) by the hadronic branch. With increasing  $V_1$ , i.e. the repulsive part in the FCM EoS, the transition point moves to larger values of the pressure and the energy density, and as a consequence we explore regions of the phase diagram where the topology changes. For instance, for  $V_1 = 0$  we can get both (B) connected and disconnected hybrid star branches, whereas for  $V_1 = 100$  MeV connected (C) hybrid star branches are present and, for the largest value of  $V_1 = 200$  MeV the hybrid branch is absent (A), and only purely nucleonic stars do exist. The additional contribution of the CFL pressure to the FCM EoS produces only a shift of the transition point, and therefore the topology explored can be different than the one of the unpaired case, leaving unchanged the phase diagram.

In Fig. 4 we display the mass-radius (left panel) and the mass-central density relation (right panel) in the case that the EoS used for the hadronic phase is the DBHF. Moreover, we observe a topology similar to the one displayed in Fig. 3, except the (B) configurations, which do not appear for the chosen set of values used for  $V_1$ ,  $G_2$  and  $\Delta$ .

Finally we comment on the values of the maximum mass. In both cases, either BHF or DBHF EoS for the hadronic matter, we see that the largest possible values of the maximum mass are obtained only for values of  $V_1 > 100$  MeV, and that only in the DBHF case maximum masses well above the observational limit are possible. In fact, the heaviest BHF+FCM hybrid star has a mass of  $2.03 M_\odot$ , and the heaviest DBHF+FCM hybrid star has a mass of  $2.31 M_\odot$ . Those values are indicated by an orange cross in Fig. 5, where we display the mapping between the FCM and CSS parameters which are, in addition to the particular constant value of the speed of sound  $c_{QM}$ , the ratio of the pressure and energy density in nuclear matter,  $p_{trans}/\epsilon_{trans}$ , and the ratio of the energy density discontinuity at the transition and the energy density at the transition,  $\Delta\epsilon/\epsilon_{trans}$ . In the upper (lower) panels we show results for the BHF (DBHF) hadronic EoS, whereas in the left, middle and right panels calculations are reported for different values of the gap  $\Delta = 0, 50, 100$  MeV respectively. The solid red line shows the threshold value  $\Delta\epsilon_{crit}$  below which there is always a stable hybrid star branch connected to the neutron star branch. This critical value is given by [61, 62, 63]

$$\frac{\Delta\epsilon_{crit}}{\epsilon_{trans}} = \frac{1}{2} + \frac{3}{2} \frac{p_{trans}}{\epsilon_{trans}} \quad (19)$$

and is obtained by performing an expansion in powers of the size of the core of the high-density phase. That result is analytical and independent on both  $c_{QM}^2$  and

**Table 1.** The minimum and maximum values of  $G_2$  (in units of GeV<sup>4</sup>) are shown for different choices of  $\Delta$  and  $V_1$ .

$\Delta$ (MeV)	$V_1$ (MeV)	$G_2^{min}$	$G_2^{max}$
0.	-50.	0.007	0.014
	0.	0.005	0.012
	100.	0.003	0.01
	200.	0.003	0.01
100.	-50.	0.009	0.014
	0.	0.007	0.012
	100.	0.006	0.01
	200.	0.003	0.01

the hadronic EoS. The solid (dashed) green lines represent the phase boundaries for connected and disconnected branches, and are obtained for  $c_{QM}^2 = 1/3(0.28)$ . Those values span the range of  $c_{QM}^2$  relevant for the FCM, as discussed in [22]. The dashed black contour delimit the region accessible by the FCM calculation. Above that region, the symbols connected by solid lines show the CSS parameterization of the FCM quark matter EoS. Along each line we keep  $V_1$  constant and vary  $G_2$  over the range indicated in Table 1 for the two extreme cases  $\Delta = 0, 100$  MeV and different values of  $V_1$ , for both BHF and DBHF. In Fig. 5  $V_1$  varies from -50 MeV up to the maximum value at which hybrid star configurations occur, which is indicated by an (orange) cross. For the BHF case that value is  $V_1 = 240$  MeV,  $G_2 = 0.0024$  GeV<sup>4</sup> and for the DBHF case it is  $V_1 = 255$  MeV,  $G_2 = 0.0019$  GeV<sup>4</sup>. The vertical black dashed lines indicate the parameter regions accessible by the FCM and consistent with the measurement of a  $M = 2 M_\odot$ . Hybrid stars with mass heavier than  $2 M_\odot$  lie on a very small connected branch on the right side of the vertical black dashed lines, and cover a small range of central pressures, having a very tiny quark core, with mass and radius similar to those of the heaviest purely hadronic star, as was already discussed in Ref. [22]. Moreover we notice that along each line of constant  $V_1$ ,  $p_{trans}/\epsilon_{trans}$  grows with  $G_2$ , and this can be explained by recalling the linear dependence of the quark pressure on  $G_2$  in Eq. (10), so that, at fixed chemical potential, an increase of  $G_2$  lowers the quark pressure, making quark matter less favourable, and shifting the transition point to higher chemical potential or pressure. This was already discussed in Ref. [19] for BHF nuclear matter, and is equally applicable to DBHF nuclear matter. We also see in Fig. 5 that an increase of  $V_1$  moves the curves slightly downward and to the right. This is expected since  $V_1$  is a measure of the interparticle repulsion, and therefore it is inversely proportional to the pressure of the system, so the pressure decreases as  $V_1$  is increased at fixed  $\mu_B$ , and, as already discussed for the parameter  $G_2$ , a decrease of the quark pressure raises  $p_{trans}$ . Fig. 5 shows that the introduction of a color-flavor locking effect characterized by a gap  $\Delta$  does not change qualitatively the gross features of the phase transition, though the topology of the hybrid star branch is slightly affected.



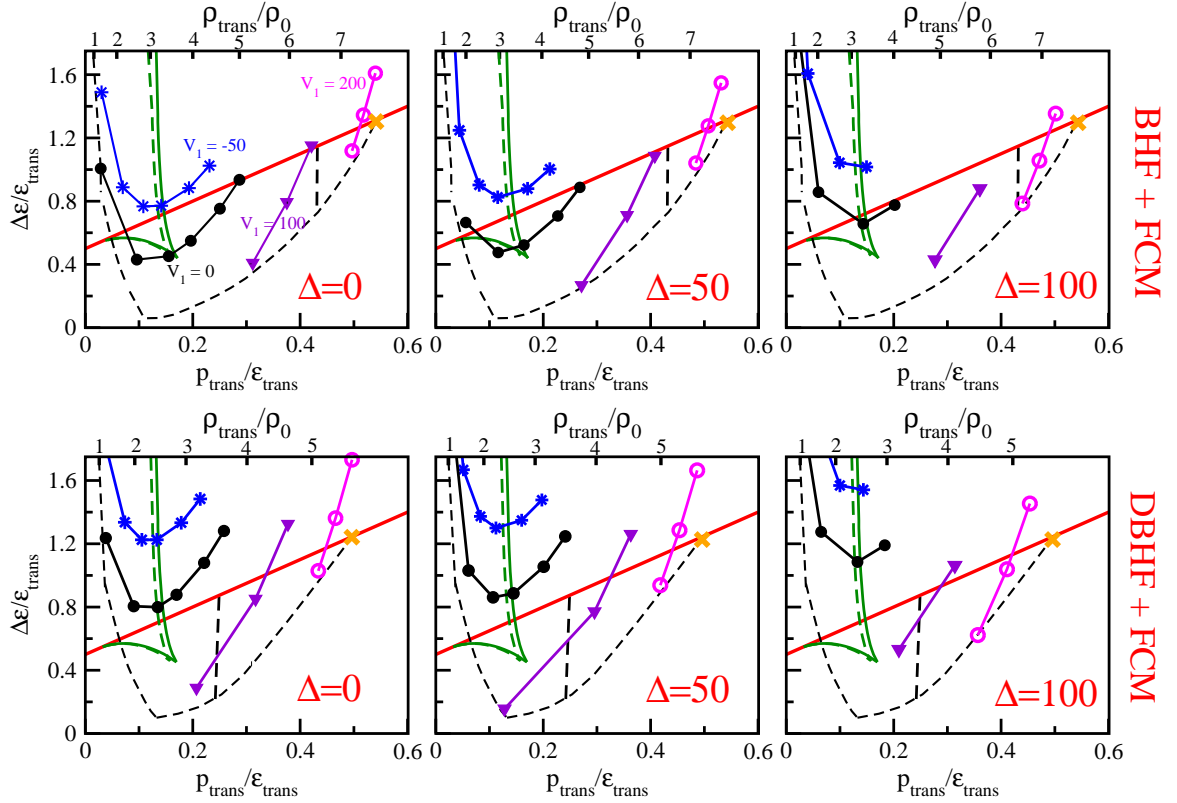


**Fig. 5.** The mapping of the FCM quark matter model onto the CSS parameterization. Results are obtained using the BHF (upper panels) and DBHF (lower panels) nuclear matter EoS. The green curves are the phase boundaries for the occurrence of connected and disconnected hybrid branches. The dashed black line delimit the region yielded by the FCM model. Within that region, the symbols give CSS parameter values for FCM quark matter as  $G_2$  is varied at constant  $V_1$  (given in MeV). The (orange) cross denotes the EoS with the highest  $p_{trans}$ , which gives the heaviest FCM hybrid star. The left, middle, and right panels display results obtained with  $\Delta = 0, 50$ , and  $100$  MeV respectively.

### 4.3 Effects of hyperons on the phase transition

It is known that the effect of including hyperons in the hadronic EoS is to soften the interior of the NS so that it becomes difficult to get masses of the stars as heavy as 2 solar masses. In our analysis, this is confirmed by the pressure obtained for the two parameterizations NSC89 and ESC08, which are plotted in Fig. 6 (respectively, dashed and dotted black curves) together with the BHF EoS (solid black curve) used in Sect. 4.1. In fact, the steeper black curve with  $\mu_B$  of the former two curves with respect to the latter is an indication of the greater stiffness of the EoS when hyperons are neglected. At the same time we notice that the NSC89 and ESC08 parameterizations quantitatively give very close results.

Then, it is easy to realise that the inclusion of hyperons puts more stringent constraints on the parameters of the quark matter EoS, in order to observe a crossing of the pressures in the two phases. In Fig. 6 we report four examples of quark matter pressure for different choices of the parameters (curves (a),(b),(c),(d)). These curves explicitly show that the parameter  $V_1$  is mainly responsible for their slope, while  $\Delta$  has a much smaller effect and  $G_2$ , being an additive constant to the pressure as shown in Eq.

(10), produces a global upward or downward shift of the quark matter pressure.

Therefore, when going from  $V_1 = -50$  MeV to  $V_1 = 0$  to  $V_1 = 120$  MeV, the corresponding curves (a), (b) and (c) become less and less steep, and one can observe three representative behaviors: (a) shows a phase transition at a crossing point below 1100 MeV with any hadronic EoS; (b) has the same crossing as in the case (a) and, when compared to the BHF EoS, it remains the favoured phase at any  $\mu_B$ , but when compared to the NSC89 or ESC08 parameterizations, one observes a second crossing at larger  $\mu_B$ ; (c), after an interval in which the pressures for the hadronic and quark phases are substantially the same, the NSC89 or ESC08 curves stay above (c) which, in turn is above the BHF curve.

Therefore, one learns that the quark pressure can exceed the pressure of hadronic EoS including hyperons only at small  $V_1$ , typically well below 100 MeV, and one knows from the analysis of Sect. 4.2 that smaller  $V_1$  correspond to NS with smaller masses. To verify this point, we consider the cases (a) and (b) (retaining for (b) only the first crossing of the quark and hadronic pressure) and then derive the corresponding mass-radius or mass-central density relation which are given in Fig. 7 for the ESC08 EoS (the NSC89 case produces almost indistinguishable results). It

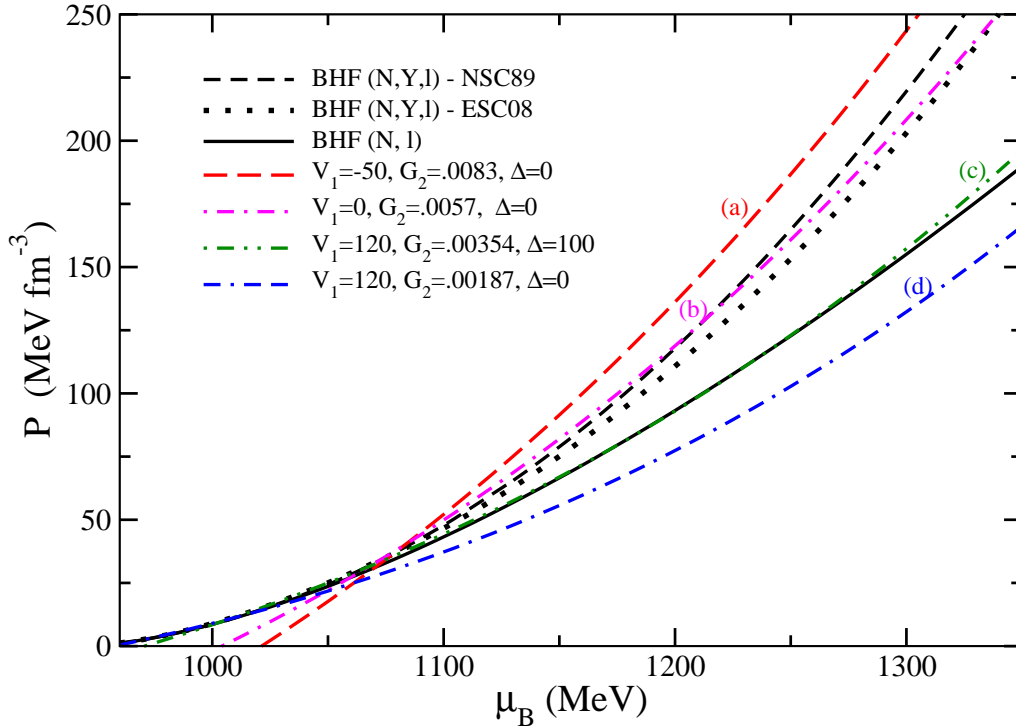


**Fig. 6.** Pressure vs. baryon chemical potential corresponding to the hadronic EoS's, including hyperons (dashed and dotted black lines) or without hyperons (BHF) (dot-dashed black line), and their crossing with the quark matter pressure evaluated with four different parameterisations ((a),(b),(c),(d)) lines.

is evident that in the cases (a) and (b), the masses remain below  $1.5 M_{\odot}$ . In addition, for (b) we ignored the second crossing point above which, in principle, the hadronic phase becomes again favourable, but, in any case, this new transition would make the NS even softer thus lowering its maximum mass and ruling out the possibility of reaching  $2 M_{\odot}$ .

Before concluding, we reconsider in some other cases the procedure followed for (b), namely the derivation of the mass-radius relation obtained by systematically considering only the transition from hadronic to quark matter occurring at the lowest value of  $\mu_B$ , while ignoring other potential transitions occurring at higher  $\mu_B$ .

By following this procedure, which is somehow justified by our poor knowledge of the hyperon interactions, we reconsider in detail the various examples of Fig. 6 and, for convenience, we report in Fig. 8 an enlargement of the region at small  $\mu_B$ . In fact, from Fig. 8 it is evident that the double transition which is observed at a larger scale in Fig. 6 for the case (b), now occurs on a smaller scale for the cases (c) and (d). These two examples are realized with  $V_1 = 120$  MeV and, respectively,  $\Delta = 100$  MeV and  $\Delta = 0$  and  $G_2$  is tuned to make the quark matter pressure almost tangent to the NSC89 or ESC08. While the case (c) crosses for the first time the hadronic EoS's slightly above  $\mu_B \sim 1000$  MeV, where the ESC08 and the BHF EoS's are distinguishable, the crossing of curve (d) occurs below  $\mu_B \sim 800$  MeV, before the onset of hyperons.

In both cases (c) and (d), the second crossing is very close, but according to the assumption made we retain

only the quark matter EoS at larger  $\mu_B$  after the first crossing. The interesting point is that, as  $V_1 = 120$  MeV is rather large for these two cases, one expects large maximum masses for the corresponding NS. This can be verified by looking at the right panel of Fig. 7, where after a very small plateau, related to the small difference between the quark and hadronic pressure along a rather large interval around the transition point, the mass of the NS grows above  $1.7 M_{\odot}$  for (c) and up to  $1.95 M_{\odot}$  for (d) that is reasonably close to the observational constraint of  $2 M_{\odot}$ . It is remarkable that very similar results are obtained for the maximum NS masses in [64] where the NSC89 parameterization is used for hyperons and a sort of QCD corrected bag model for quark matter.

## 5 Conclusions

The FCM extension at finite  $T$  and  $\mu_B$  provides us a very simple description of the quark dynamics in terms of two parameters, namely the gluon condensate  $G_2$ , that parametrizes the vacuum pressure and energy density, and hence is strictly related to the bag constant of the MIT bag model, and the potential  $V_1$ , which summarises the interaction corrections to the free quark and gluon pressure. It is then natural to explore the predictions of the FCM on the maximum masses (and their associated radii) of NS when these parameters are varied. In order to have a more complete picture, we include the effect of color superconductivity through the CFL mechanism, which amounts to

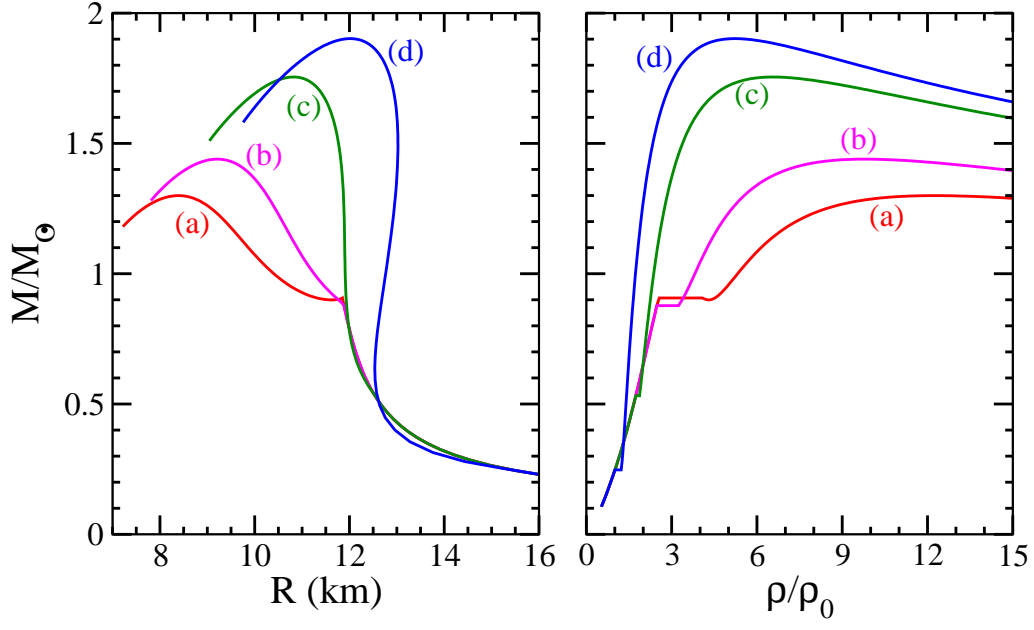


**Fig. 7.** Mass-radius (left panel) and mass-central density (right panel) plots of the hybrid stars corresponding to the quark matter EoS (a), (b), (c), (d) together with the hyperon parameterization ESC08 of Fig. 6.

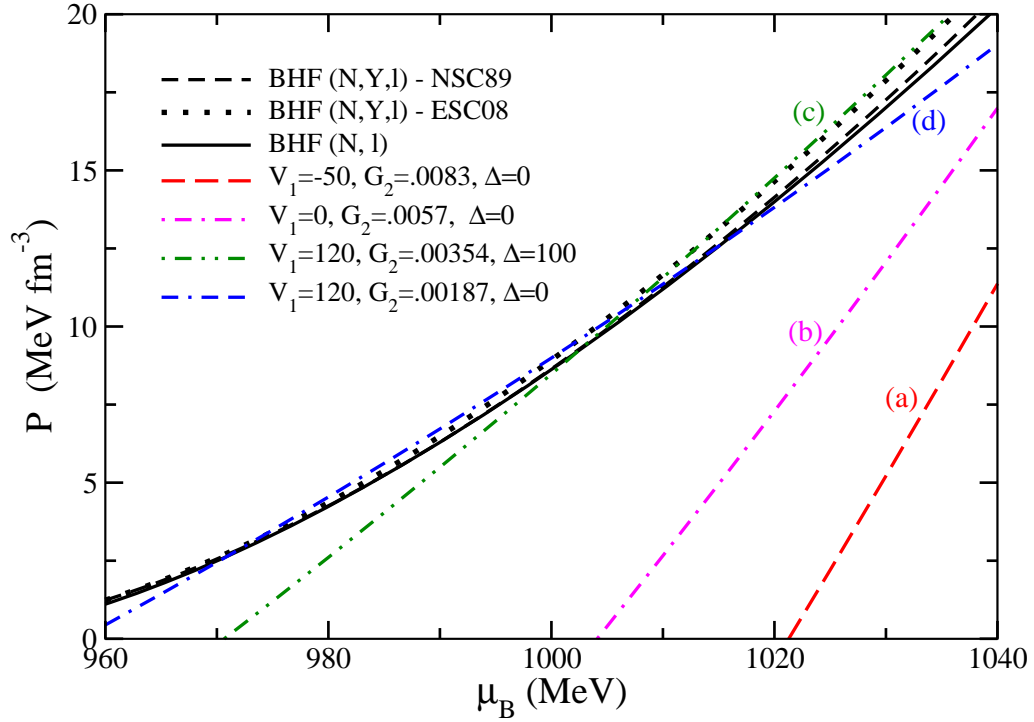


**Fig. 8.** Enlargement of the low  $\mu_B$  region of Fig. 6.

the addition of a new free energy contribution written in terms of the gap  $\Delta$ .

Clearly, any prediction of a quark matter model on the structure of a hybrid NS strongly depends on the nuclear matter EoS employed and among the large variety of nuclear EoS available in the literature, we focused on the non-relativistic BHF EoS and its relativistic counterpart, the DBHF EoS. These are derived within a solid microscopic approach, and give us different predictions on the NS maximum mass. For completeness, we also analyzed the inclusion of the hyperon degrees of freedom that produces a softening of the nuclear matter EoS with the consequent reduction of the maximum mass of the NS.

With this new set of more refined calculations, we confirm the trend already observed in [19,20,22], i.e. the maximum mass of hybrid stars grows with the two parameters  $V_1$  and  $G_2$  while it decreases when  $\Delta$  is increased. More interestingly, we extend the mapping developed in [22] among the parameters of the FCM and those defining the CSS parameterization, by displaying the effect of the gap  $\Delta$ . In fact, from the various panels of Fig. 5, it is evident that the border of the area of the diagram accessible by the FCM (i.e. the dashed black curve) is not sensitive to  $\Delta$  and it is totally determined in terms of the CSS parameters. In particular, even the region corresponding to configurations associated to hybrid stars with maximum mass greater than  $2 M_\odot$ , which is the triangle-like area delimited above by the straight solid red line, below by the dashed black curve and finally on the left by the almost vertical dashed black segment, is only determined in terms of the two CSS parameters reported on the  $x$  and  $y$  axes of the diagrams. Therefore one can conclude that a particular configuration with mass around or above two solar masses can be realized in the FCM by different pairs of  $G_2$  and  $V_1$ , depending on the specific value assigned to  $\Delta$ , i.e. the appearance of a color superconducting gap can be mimicked by a shift of the other two parameters. Therefore, even the mass of the heaviest hybrid star predicted by the FCM (the orange crosses in Fig. 5) does not correspond to a unique set of  $G_2$ ,  $V_1$  and  $\Delta$ , while, as seen in [22], its value strongly depends on the specific choice made for the nuclear matter EoS.

Instead, the inclusion of the hyperons induces dramatic changes in this picture. In fact, a regular transition from nuclear to quark matter with a stable quark phase up to very high chemical potential requires a particular tuning of the FCM parameters that leads to very low maximum masses, below  $1.5 M_\odot$ . We have also observed that it is possible to find specific sets of the parameters  $G_2$ ,  $V_1$  and  $\Delta$  such that the hadronic and quark matter pressure run very close for a large range of  $\mu_B$  and, when looking more in detail, one observes multiple crossings of these lines, although at large  $\mu_B$  the phase that includes hyperons is favoured. For completeness we analyze these cases by retaining only the first crossing from the hadronic to the quark matter phase, and neglecting the other transitions at higher chemical potential. In this case it is possible to tune the FCM parameters in such a way to raise the maximum mass up to  $1.95 M_\odot$ , although an explanation

supporting the strong assumption on the transition is required in order to accept this result.

## Acknowledgments

We thank H.-J. Schulze (INFN Sezione di Catania) for providing us with the BHF EoS for hypernuclear matter with the NSC89 and ESC08 nucleon-hyperon parameterizations. We are also grateful to M. Alford for bringing the CSS parameterization to our attention. Partial support comes from “NewCompStar”, COST Action MP1304.

## References

1. N. K. Glendenning, ed., *Compact stars : nuclear physics, particle physics, and general relativity*, 2000.
2. P. B. Demorest, T. Pennucci, S. M. Ransom, M. S. E. Roberts, and J. W. T. Hessels, *A two-solar-mass neutron star measured using Shapiro delay*, *Nature* **467** (2010) 1081–1083, [[arXiv:1010.5788](#)].
3. J. Antoniadis, P. Freire, N. Wex, T. Tauris, R. Lynch, and et al., *A Massive Pulsar in a Compact Relativistic Binary*, *Science* **340** (2013) 1233232, [[arXiv:1304.6875](#)].
4. M. Baldo, I. Bombaci, and G. Burgio, *Microscopic nuclear equation of state with three-body forces and neutron star structure*, *Astron.Astrophys.* **328** (1997) 274–282, [[astro-ph/9707277](#)].
5. A. Akmal, V. R. Pandharipande, and D. G. Ravenhall, *Equation of state of nucleon matter and neutron star structure*, *Phys. Rev. C* **58** (Sept., 1998) 1804–1828, [[nucl-th/9804027](#)].
6. X. R. Zhou, G. F. Burgio, U. Lombardo, H.-J. Schulze, and W. Zuo, *Three body forces and neutron star structure*, *Phys.Rev.* **C69** (2004) 018801.
7. M. Baldo, A. Polls, A. Rios, H.-J. Schulze, and I. Vidana, *Comparative study of neutron and nuclear matter with simplified Argonne nucleon-nucleon potentials*, *Phys.Rev.* **C86** (2012) 064001, [[arXiv:1207.6314](#)].
8. Z. Li, U. Lombardo, H.-J. Schulze, and W. Zuo, *Consistent nucleon-nucleon potentials and three-body forces*, *Phys.Rev.* **C77** (2008) 034316.
9. P. de-Forcrand, *Simulating QCD at finite density*, in *Symposium on Lattice Field Theory*, p. 10, 2009.
10. Y. Aoki, G. Endrődi, Z. Fodor, S. D. Katz, and K. K. Szabó, *The order of the quantum chromodynamics transition predicted by the standard model of particle physics*, *Nature* **443** (2006) 675–678, [[hep-lat/0611014](#)].
11. A. Bazavov, T. Bhattacharya, M. Cheng, N. H. Christ, C. Detar, S. Ejiri, S. Gottlieb, R. Gupta, U. M. Heller, K. Huebner, C. Jung, F. Karsch, E. Laermann, L. Levkova, C. Miao, R. D. Mawhinney, P. Petreczky, C. Schmidt, R. A. Soltz, W. Soeldner, R. Sugar, D. Toussaint, and P. Vranas, *Equation of state and QCD transition at finite temperature*, *Phys. Rev. D* **80** (2009), no. 1 014504, [[arXiv:0903.4379](#)].
12. G. F. Burgio, M. Baldo, P. K. Sahu, and H.-J. Schulze, *Hadron-quark phase transition in dense matter and neutron stars*, *Phys. Rev. C* **66** (2002), no. 2 025802, [[nucl-th/0206009](#)].

13. M. Baldo, M. Buballa, G. F. Burgio, F. Neumann, M. Oertel, and H.-J. Schulze, *Neutron stars and the transition to color superconducting quark matter*, Physics Letters B **562** (2003) 153–160, [nuc1-th/0212096].
14. C. Maieron, M. Baldo, G. F. Burgio, and H.-J. Schulze, *Hybrid stars with the color dielectric and the MIT bag models*, Phys. Rev. D **70** (2004), no. 4 043010, [nuc1-th/0404089].
15. H. Chen, M. Baldo, G. F. Burgio, and H.-J. Schulze, *Hybrid stars with the Dyson-Schwinger quark model*, Phys. Rev. D **84** (2011), no. 10 105023, [arXiv:1107.2497].
16. H. G. Dosch, *Gluon Condensate and Effective Linear Potential*, Phys.Lett. **B190** (1987) 177.
17. H. G. Dosch and Y. Simonov, *The Area Law of the Wilson Loop and Vacuum Field Correlators*, Phys.Lett. **B205** (1988) 339.
18. Y. Simonov, *Vacuum Background Fields in QCD as a Source of Confinement*, Nucl.Phys. **B307** (1988) 512.
19. M. Baldo, G. Burgio, P. Castorina, S. Plumari, and D. Zappalà, *Astrophysical constraints on the confining models: The Field Correlator Method*, Phys.Rev. **D78** (2008) 063009, [arXiv:0804.2328].
20. S. Plumari, G. Burgio, V. Greco, and D. Zappalà, *Quark matter in Neutron Stars within the Field Correlator Method*, Phys.Rev. **D88** (2013), no. 8 083005, [arXiv:1307.3055].
21. M. G. Alford, S. Han, and M. Prakash, *Generic conditions for stable hybrid stars*, Phys.Rev. **D88** (2013), no. 8 083013, [arXiv:1302.4732].
22. M. G. Alford, G. F. Burgio, S. Han, G. Taranto, and D. Zappalà, *Constraining and applying a generic high-density equation of state*, ArXiv e-prints (2015) [arXiv:1501.0790].
23. M. Baldo, ed., *Nuclear Methods and The Nuclear Equation of State*. World Scientific, Singapore, 1999.
24. T. Gross-Boelting, C. Fuchs, and A. Faessler, *Covariant representations of the relativistic Bruckner  $T$  matrix and the nuclear matter problem*, Nucl.Phys. **A648** (1999) 105–137, [nuc1-th/9810071].
25. H. Song, M. Baldo, G. Giansiracusa, and U. Lombardo, *Bethe-Brueckner-Goldstone Expansion in Nuclear Matter*, Phys.Rev.Lett. **81** (1998) 1584–1587.
26. M. Baldo, A. Fiasconaro, H. Q. Song, G. Giansiracusa, and U. Lombardo, *High density symmetric nuclear matter in the Bethe-Brueckner-Goldstone approach*, Phys.Rev. **C65** (2002) 017303.
27. B. Day, *Three-body correlations in nuclear matter*, Phys.Rev. **C24** (1981) 1203–1271.
28. M. Baldo and K. Fukukawa, *Nuclear Matter from Effective Quark-Quark Interaction*, Physical Review Letters **113** (2014), no. 24 242501, [arXiv:1409.7206].
29. J. Carlson, V. Pandharipande, and R. B. Wiringa, *Three-nucleon interaction in 3-body, 4-body, and infinite-body systems*, Nucl.Phys. **A401** (1983) 59–85.
30. R. Schiavilla, V. Pandharipande, and R. B. Wiringa, *Momentum distributions in a  $A = 3$  and 4 nuclei*, Nucl.Phys. **A449** (1986) 219–242.
31. Z. Li and H. Schulze, *Nuclear matter with chiral forces in Brueckner-Hartree-Fock approximation*, Phys.Rev. **C85** (2012) 064002.
32. M. Baldo, G. Burgio, and H. Schulze, *Onset of hyperon formation in neutron star matter from Brueckner theory*, Phys.Rev. **C58** (1998) 3688–3695.
33. M. Baldo, G. Burgio, and H. Schulze, *Hyperon stars in the Brueckner-Bethe-Goldstone theory*, Phys.Rev. **C61** (2000) 055801, [nuc1-th/9912066].
34. P. M. M. Maessen, T. A. Rijken, and J. J. de Swart, *Soft-core baryon-baryon one-boson-exchange models. II. Hyperon-nucleon potential*, Phys. Rev. (1989) 2226–2245.
35. V. G. J. Stoks and T. A. Rijken, *Soft-core baryon-baryon potentials for the complete baryon octet*, Phys. Rev. (1999) 3009–3020, [nuc1-th/9901028].
36. H.-J. Schulze and T. Rijken, *Maximum mass of hyperon stars with the Nijmegen ESC08 model*, Phys. Rev. (2011), no. 3 035801.
37. G. Brown, W. Weise, G. Baym, and J. Speth, *The equation of state of dense matter*, Comm. Nucl. Part. Phys. **17** (1987) 39–50.
38. M. Baldo, G. Giansiracusa, U. Lombardo, I. Bombaci, and L. S. Ferreira, *Microscopic theory of the Nuclear Equation of State*, Nuclear Physics A **583** (1995) 599–606.
39. Z. H. Li, U. Lombardo, H.-J. Schulze, W. Zuo, L. W. Chen, and H. R. Ma, *Nuclear matter saturation point and symmetry energy with modern nucleon-nucleon potentials*, Phys.Rev. **74** (2006), no. 4 047304.
40. A. Di Giacomo, H. G. Dosch, V. Shevchenko, and Y. Simonov, *Field correlators in QCD: Theory and applications*, Phys.Rept. **372** (2002) 319–368, [hep-ph/0007223].
41. Y. Simonov and M. Trusov, *Deconfinement transition for nonzero baryon density in the field correlator method*, JETP Lett. **85** (2007) 598–601, [hep-ph/0703228].
42. Y. Simonov and M. Trusov, *Vacuum phase transition at nonzero baryon density*, Phys.Lett. **B650** (2007) 36–40, [hep-ph/0703277].
43. A. Nefediev, Y. Simonov, and M. Trusov, *Deconfinement and quark-gluon plasma*, Int.J.Mod.Phys. **E18** (2009) 549–599, [arXiv:0902.0125].
44. M. A. Shifman, A. Vainshtein, and V. I. Zakharov, *QCD and Resonance Physics. Sum Rules*, Nucl.Phys. **B147** (1979) 385–447.
45. M. A. Shifman, A. Vainshtein, and V. I. Zakharov, *QCD and Resonance Physics: Applications*, Nucl.Phys. **B147** (1979) 448–518.
46. M. D’Elia, A. Di Giacomo, and E. Meggiolaro, *Field strength correlators in full QCD*, Phys.Lett. **B408** (1997) 315–319, [hep-lat/9705032].
47. M. D’Elia, A. Di Giacomo, and E. Meggiolaro, *Gauge invariant field strength correlators in pure Yang-Mills and full QCD at finite temperature*, Phys.Rev. **D67** (2003) 114504, [hep-lat/0205018].
48. I. Bombaci and D. Logoteta, *A link between measured neutron star masses and lattice QCD data*, Monthly Notices of the Royal Astronomical Society - Letters, Vol. 433, **L79-L83** (2013) [arXiv:1212.5907].
49. T. D. Cohen, R. Furnstahl, and D. K. Griegel, *Quark and gluon condensates in nuclear matter*, Phys.Rev. **C45** (1992) 1881–1893.
50. E. Drukarev, M. Ryskin, and V. Sadovnikova, *QCD condensates and hadron parameters in nuclear matter: Selfconsistent treatment, sum rules and all that*, Prog.Part.Nucl.Phys. **47** (2001) 73–139, [nuc1-th/0106049].
51. M. Baldo, P. Castorina, and D. Zappalà, *Gluon condensation and deconfinement critical density in nuclear matter*, Nucl.Phys. **A743** (2004) 3–12, [nuc1-th/0311038].

52. M. A. Metlitski and A. R. Zhitnitsky, *Theta-parameter in 2 color QCD at finite baryon and isospin density*, Nucl.Phys. **B731** (2005) 309–334, [[hep-ph/0508004](#)].
53. A. Zhitnitsky, *Vacuum energy, EoS, and the gluon condensate at finite baryon density in QCD*, AIP Conf.Proc. **892** (2007) 518–520, [[hep-ph/0701065](#)].
54. M. G. Alford, K. Rajagopal, and F. Wilczek, *Color flavor locking and chiral symmetry breaking in high density QCD*, Nucl.Phys. **B537** (1999) 443–458, [[hep-ph/9804403](#)].
55. M. G. Alford, A. Schmitt, K. Rajagopal, and T. Schfer, *Color superconductivity in dense quark matter*, Rev.Mod.Phys. **80** (2008) 1455–1515, [[arXiv:0709.4635](#)].
56. K. Rajagopal and F. Wilczek, *Enforced electrical neutrality of the color flavor locked phase*, Phys.Rev.Lett. **86** (2001) 3492–3495, [[hep-ph/0012039](#)].
57. M. Alford and K. Rajagopal, *Absence of two flavor color superconductivity in compact stars*, JHEP **0206** (2002) 031, [[hep-ph/0204001](#)].
58. M. Alford, M. Braby, M. Paris, and S. Reddy, *Hybrid stars that masquerade as neutron stars*, Astrophys.J. **629** (2005) 969–978, [[nucl-th/0411016](#)].
59. S. L. Shapiro and S. A. Teukolsky, *Black Holes, White Dwarfs and Neutron Stars: The Physics of Compact Objects*. 1986.
60. J. W. Negele and D. Vautherin, *Neutron star matter at sub-nuclear densities*, Nuclear Physics A **207** (1973) 298–320.
61. R. Schaeffer, L. Zdunik, and P. Haensel, *Phase transitions in stellar cores. I - Equilibrium configurations*, Astron. Astrophys. **126** (1983) 121–145.
62. Z. F. Seidov, *The Stability of a Star with a Phase Change in General Relativity Theory*, Sov. Astron. **15** (1971) 347.
63. L. Lindblom, *Phase transitions and the mass radius curves of relativistic stars*, Phys.Rev. **D58** (1998) 024008, [[gr-qc/9802072](#)].
64. A. Kurkela, P. Romatschke, and A. Vuorinen, *Cold Quark Matter*, Phys.Rev. **D81** (2010) 105021, [[arXiv:0912.1856](#)].